Thermodynamic Analysis of the Structural Stability of the Shiga Toxin B-Subunit†

David G. Pina,‡ Javier Gómez,§ Enrique Villar,‡ Ludger Johannes,|| and Valery L. Shnyrov*,‡

Departamento de Bioquímica y Biología Molecular, Universidad de Salamanca, 37007 Salamanca, Spain, Instituto de Biología Molecular y Celular, Universidad Miguel Hernández, 03202 Elche−Alicante, Spain, and Laboratoire Trafic et Signalisation, Institut Curie, UMR 144 Curie/CNRS, 75248 Paris Cedex 05, France

Received April 14, 2003; Revised Manuscript Received June 10, 2003

ABSTRACT: The conformational stability of Shiga toxin B-subunit (STxB), a pentameric protein from *Shigella dysenteriae* has been characterized by high sensitivity differential scanning calorimetry and circular dichroism spectroscopy under different solvent conditions. It is shown that the thermal folding/unfolding of STxB is a reversible process involving a highly cooperative transition between folded pentamer and unfolded monomers. The conformational stability of STxB is pH dependent and because of its pentameric nature is also concentration dependent. STxB is maximally stable in the pH range from 5 to 9 (ΔG upon unfolding is close to 13 kcal per mol of monomer at 25 °C), and its stability decreases both at lower and at higher pH values. The pH dependence of the Gibbs energy of stabilization between pH 2.5 and 5 is consistent with the change in the ionizable state of an average of four groups per monomer upon unfolding. Structural thermodynamic calculations show that the stabilization of the STxB pentamer is primarily due to the interactions established between monomers rather than intramonomer interactions. The folding of an isolated monomer into the conformation existing in the pentamer is unfavorable and expected to be characterized by a free-energy change upon folding in the order of 2.5 kcal mol^{-1} at 25 °C. On the average, intersubunit interaction induced upon oligomerization of folded monomers should contribute close to −13.4 kcal per mol of monomer to bring the overall Gibbs energy to the experimentally determined value at this temperature.

Shiga toxin—produced by *Shigella dysenteriae*—and the related verotoxins—produced by certain enterohemorrhagic *Escherichia coli* strains—are proteins belonging to the AB_5 bacterial toxin family, which also comprises cholera and pertussis toxin and whose morphology consists of two noncovalently associated subunits (*1*, *2*). The A-subunit displays ribosomal RNA *N*-glycanase activity responsible for the inhibition of protein biosynthesis but is unable to enter cells by itself. Toxin cell-surface recognition and internalization requires interaction with the B-subunit (STxB).[1] This association does not alter the structure of the latter, and it seems that holotoxin and STxB alone bind to cells and are transported in essentially the same manner (*3*). STxB is a nonglycosylated homopentameric protein composed of monomers of 69 residues (7.7 kDa), each with one disulfide bond. Its specific cell-surface receptor is a glycosphingolipid called globotriaosylceramide (Gb_3). Thus, STxB monomers are among the smallest known lectins. The toxin−receptor complex is internalized via clathrin-dependent and/or -independent endocytosis, and STxB is then transported in a process involving membrane microdomains from the early endosome to the ER, via the *trans*-Golgi network and Golgi apparatus, a pathway known as retrograde transport (*4*−*9*). Transport to the ER is believed to be necessary for translocation to the cytosol of the holotoxin to perform its biological function (*10*, *11*). Alone, STxB has no toxic activity and is currently used as a tool in research into intracellular transport pathways, namely, in the study of the retrograde transport route, and in the field of medicine, as a vector for immunotherapeutic antitumor response, since a number of characteristics predispose the molecule for use in antigen presentation (*12*). Understanding the mechanism of entry of this protein into cells is therefore of fundamental importance from both the academic and the applied points of view.

The crystal structure of STxB and holotoxin have both been solved (*13*−*15*). Each B-subunit monomer comprises two three-stranded antiparallel β-sheets and an α-helix (see Figure 1). The pentamer forms a ring-like structure with a central pore of about an 11 Å diameter delimited by five α-helices and surrounded by β-sheets from pairs of adjacent monomers, forming six-stranded antiparallel β-sheets. Recent studies have suggested that STxB has three Gb_3 binding sites per monomer, although only one of them would be substantially occupied by ligand in solution (*16*, *17*).

† This work was partially supported by grants from the Association pour la Recherche sur le Cancer (5177), the French Ministry of Science (ACI-5233 Jeunes Chercheurs) to L.J. and Spanish Ministry of Science and Technology (BIO2000-1089) to J.G. D.G.P. is a fellowship holder from Fundação para a Ciência e a Tecnologia, Portugal (SFRH/BD/1067/2000) and was supported by a FEBS short-term fellowship during his stay at the Curie Institute, Paris.

* To whom correspondence should be addressed. Phone: +34 923 294465. Fax: +34-923-294579. E-mail: shnyrov@usal.es.

‡ Universidad de Salamanca.

§ Universidad Miguel Hernández.

|| Institut Curie.

[1] Abbreviations: STxB, Shiga toxin B-subunit; ER, endoplasmic reticulum; DSC, differential scanning calorimetry; UV CD, ultraviolet circular dichroism; ΔG, Gibbs free energy of protein unfolding; ΔC_p, heat capacity change; Gdn-HCl, guanidine hydrochloride; ASA, accessible surface area.

10.1021/bi034591s CCC: $25.00
Published on Web 07/16/2003

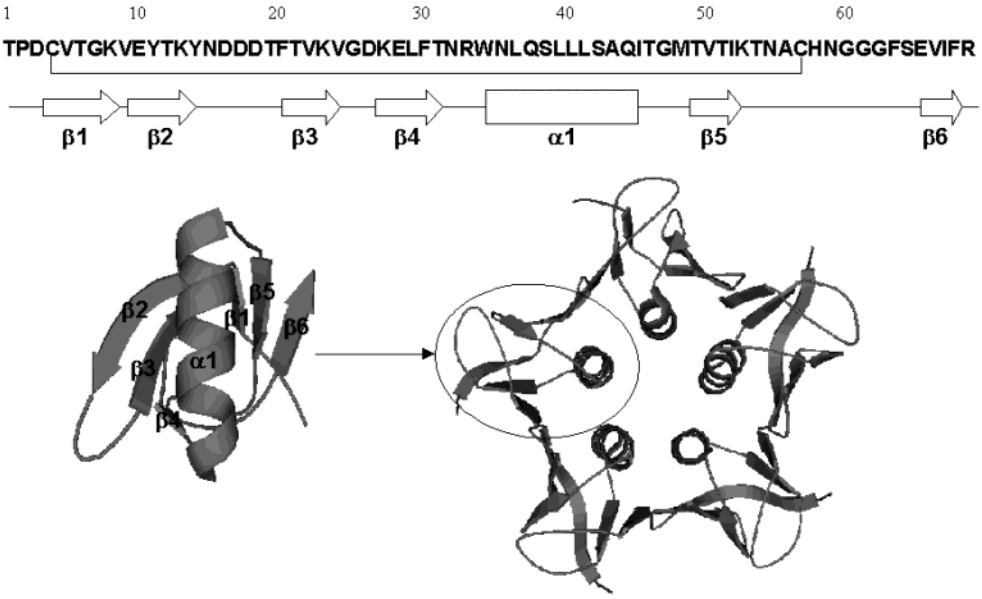

FIGURE 1: Schematic representation of STxB primary, secondary, tertiary, and quaternary structure. Interaction between monomers mainly occurs at the $\beta 2-\beta 6$ interface. The three-dimensional presentation was made using PyMOL software (PDB 1DMO).

The conformational stability of STxB has not yet been characterized. High-sensitivity differential scanning calorimetry (DSC) is the technique of choice for the study of the energetics associated with folding/unfolding reactions involving proteins, leading to the thermodynamic characterization of intermolecular recognition processes (i.e., oligomerization processes), as well as intramolecular recognition events (i.e., monomer folding) (*18*−*21*). Here, DSC, together with circular dichroism (CD), was used to determine the structural stability of STxB as a function of temperature, protein concentration, pH, and denaturant (Gdn-HCl) concentration. The results clearly show that the heat-induced unfolding of STxB is a highly cooperative, two-state reversible process in which only folded pentamers and unfolded monomers are appreciably populated along the reaction.

Structural thermodynamic analyses based on the correlations established between the structural and the energetic changes induced by inter- and intramolecular recognition processes (*22*−*25*) allow one to dissect the different contributions of the protein to the conformational stability. Such calculations reveal that the stabilization of the STxB pentamer is due to interactions established between individual subunits. The magnitude of these interactions overcomes the unfavorable Gibbs free energy change upon monomer folding. It has been shown that the conformational instability of folded monomers is due to the large entropy penalty associated with the decrease in the conformational degrees of freedom of the both backbone and the side chains of the protein upon folding, which is not compensated by the gain in solvent-related entropy induced by the release of water molecules upon burial of hydrophobic surfaces and the favorable enthalpic contributions coming from the internal van der Waals and hydrogen bonding within the folded monomer. Structurally, the conformational instability of isolated STxB monomers can be rationalized as being due to exposure of the solvent to a large amount of apolar groups that only become buried upon oligomerization.

MATERIALS AND METHODS

Materials and Chemicals. Chromatography columns were from Amersham Biosciences. Gdn-HCl, HEPES, and Tris buffer were purchased from ICN Biomedicals, Inc. Double-distilled water was used throughout. All other reagents used were of the highest purity available.

Protein Preparation. Recombinant STxB was purified as described elsewhere (*26*). Expression of recombinant STxB inserted in a pSU108 plasmid was induced by heat (4 h at 42 °C) in *Escherichia coli*. The periplasmic fraction was isolated by osmotic shock after sequential exposure of a growing bacterial suspension in sucrose solution (25% w/v) and water. After periplasmic extracts had been prepared, they were loaded on a QHP chromatography column and eluted through a linear gradient in 20 mM Tris/HCl, pH 8.0. B-subunit-containing fractions were then reloaded on an affinity column prepared with the monoclonal antibody 13C4. Protein samples were dialyzed overnight against 10 mM HEPES or phosphate buffer, pH 7.0. The purity of the samples was checked by Tris/Tricine SDS−PAGE, and protein concentrations were determined spectrophotometrically using an extinction coefficient value of 9500 M^{-1} cm^{-1} at 278 nm for the monomer (*27*).

Differential Scanning Calorimetry. DSC experiments were performed on a MicroCal MC-2D differential scanning microcalorimeter (MicroCal Inc., Northampton, MA) with cell volumes of 1.22 mL as described previously (*28*). All solutions were degassed by stirring under a vacuum prior to scanning. An overpressure of 2 atm of dry nitrogen was always kept over the liquids in the cells throughout the scans. The reversibility of the thermal transitions was checked by examining the reproducibility of the calorimetric trace in a second heating of the sample immediately after cooling from the first scan. The molar excess heat capacity curves obtained by normalization with the protein concentrations and volume of the calorimeter cell were smoothed and plotted using the Windows-based software package (ORIGIN) supplied by

MicroCal. Data were analyzed by nonlinear least-squares fitting using the two-state folding/unfolding reaction coupled to oligomerization model. This model corresponds to a situation in which the oligomeric protein made up of identical subunits obeys the following equilibrium:

$$\frac{1}{n}\mathrm{N}_n \overset{K}{\leftrightarrow} \mathrm{U} \tag{1}$$

$$K = \frac{[\mathrm{U}]}{[\mathrm{N}_n]^{1/n}} \tag{2}$$

where $[N_n]$ and [U] represent the concentration of folded oligomer and unfolded monomer, respectively, and n is the number of dissociable subunits. If α is the fraction of protein in the denatured state and $(1 - \alpha)$ is the fraction of protein in the native state, then

$$[\mathrm{N}_n] = \frac{C_\mathrm{t}(1-\alpha)}{n} \tag{3}$$

$$[\mathrm{U}] = C_\mathrm{t}\alpha \tag{4}$$

Using eqs 2−4, the equilibrium constant thus becomes

$$K = n^{1/n} C_\mathrm{t}^{(n-1)/n} \frac{\alpha}{(1-\alpha)^{1/n}} \tag{5}$$

Using eq 5 and the expressions for enthalpy change

$$\left[\frac{\mathrm{d}\ln K}{\mathrm{d}T}\right]_p = \frac{\Delta H(T)}{RT^2} \tag{6a}$$

$$\Delta H(T) = \Delta H_{1/2} + \Delta C_\mathrm{p}(T - T_{1/2}) \tag{6b}$$

where $\Delta H_{1/2}$ and ΔC_p are changes in the enthalpy and heat capacity upon unfolding, respectively. By integrating eq 6 from $T_{1/2}$, where $\alpha = 0.5$, to T, one has

$$K(T) = \frac{1}{2}\left(\frac{n}{2}\right)^{1/n} C_\mathrm{t}^{(n-1)/n} \exp\left[-\frac{\Delta H_{1/2}}{R}\left(\frac{1}{T} - \frac{1}{T_{1/2}}\right) - \frac{\Delta C_\mathrm{p}}{R}\left(1 - \frac{T_{1/2}}{T} + \ln\frac{T_{1/2}}{T}\right)\right] \tag{7}$$

Once $K(T)$ is known, then $\alpha(T)$ can be solved numerically from eq 5, and the excess heat capacity function $\langle \Delta C_\mathrm{p} \rangle$, which is simply the temperature derivative of the average excess enthalpy, can be presented as

$$\langle \Delta C_\mathrm{p} \rangle = \frac{\mathrm{d}\langle \Delta H \rangle}{\mathrm{d}T} = \frac{\mathrm{d}\alpha(T)}{\mathrm{d}T}\Delta H_{1/2} + \alpha \Delta C_\mathrm{p} \tag{8}$$

The above equations were used to fit the data and obtain the best estimates for $\Delta H_{1/2}$, ΔC_p, and $T_{1/2}$.

Circular Dichroism. CD spectra in the far-UV range (190−250 nm) were recorded on a computer-controlled Jasco J-715 CD spectropolarimeter using a 1 mm path length cuvette. The protein concentration was ca. 0.13 mg/mL. The spectra reported are averages of four scans and were all background-corrected, smoothed using J-715 noise reduction software, and converted to mean residue ellipticity ($[\Theta] = 10 M_\mathrm{res}\Theta_\mathrm{obs} l^{-1} C_\mathrm{t}^{-1}$), where $M_\mathrm{res} = 110$ is the mean residue molar mass, Θ_obs is the ellipticity measured (degrees) at wavelength λ, l is the optical path length of the cell (dm), and C_t is the protein concentration (mol dm^{-3}). For the thermal unfolding experiments, samples were heated in a jacketed cell at a rate of 60 °C/h over the 30−95 °C range, using a Neslab RT-11 programmable water bath. Changes in the structure of STxB because of unfolding were followed at 225 nm every 1 °C. Individual STxB melting curves were fitted to the following equation using a nonlinear least-squares algorithm:

$$\theta = \theta_\mathrm{N}(1 - \alpha) + \theta_\mathrm{U}\alpha \tag{9}$$

where $\theta_\mathrm{N} = a_1 + a_2 T$ and $\theta_\mathrm{U} = b_1 + b_2 T$ represent the mean values of ellipticity for the native and unfolded conformations, respectively, obtained by linear regression of pre- and post-transitional baselines.

Structural Thermodynamic Calculations. The crystal structure of StxB has been solved at 2.50 Å resolution (*15*) and was used here to perform structure-based thermodynamic calculations to dissect the structural stability of the protein and to identify the different contributions to the stabilization of its pentameric structure. The Gibbs free energy change, ΔG, related to the molecular recognition process (either intramolecular, as in the case of monomer folding, or intermolecular, as in the case of its oligomerization) is decomposed into intrinsic and ionic components:

$$\Delta G = \Delta G_\mathrm{int} + \Delta G_\mathrm{ion} \tag{10}$$

where ΔG_int accounts for the contributions associated with the formation of secondary and tertiary structures (van der Waals interactions, hydrogen bonding, hydration and conformational entropy), and ΔG_ion accounts for the contributions to the free energy because of changes in the ionization states of ionizable groups coupled to the molecular recognition process.

The calculations as performed here do not include any protonation-linked effects and are thus only comparable with the experimentally determined energetics around neutral pH, where ΔG upon pentamer unfolding was seen to contain no contribution from protonation/ionization: ($\partial \Delta G/\partial \mathrm{pH} = 0$, see Figure 7).

ΔG_int was calculated from independent computation of its enthalpic and entropic components ($\Delta G = \Delta H - T\Delta S$) following the structural parametrization of the energetics involved in molecular recognition processes developed by Freire and co-workers (*22*−*25*). Central to these calculations is the value of the heat capacity change, ΔC_p, which defines the temperature dependence of ΔG as well as that of its components ΔH and ΔS. ΔC_p arises mainly from the hydration of the protein groups that become exposed to the solvent upon unfolding and has been shown to scale with the changes in the accessible surface area, ASA, induced by the molecular recognition process (*22*, *23*, *29*, *30*)

$$\Delta C_\mathrm{p} = 0.45\Delta \mathrm{ASA}_\mathrm{apolar} - 0.26\Delta \mathrm{ASA}_\mathrm{polar} \tag{11}$$

where the parameters are in units of cal K^{-1} mol^{-1} Å^{-1}.

Similarly, it has been shown (*22*, *24*) that the enthalpy change upon protein unfolding arising from changes in the hydration of protein groups as well as the breaking of internal noncovalent interactions can be calculated by changes in

ASA of both polar and apolar groups

$$\Delta H(60\ ^\circ\mathrm{C}) = -8.44\Delta\mathrm{ASA}_{\mathrm{apolar}} + 31.4\Delta\mathrm{ASA}_{\mathrm{polar}} \quad (12)$$

where the coefficients are given in units of cal mol^{-1} Å^{-1}. Other contributions to the enthalpy change upon unfolding (such as proton transfer) must be accounted for if they are coupled to the unfolding or dissociation process (*22*, *31*), as is the case of STxB unfolding at pHs both below and above neutrality (see Figure 7).

The enthalpy change at any other temperature can be calculated combining eqs 11 and 12

$$\Delta H(T) = \Delta H(60\ ^\circ\mathrm{C}) + \Delta C_{\mathrm{p}}(T - 60) \quad (13)$$

In the absence of proton-transfer coupled to the folding/unfolding reaction, the total entropy change upon folding, $\Delta S(T)$, can be assumed to comprise three terms: (i) a solvent-related term, ΔS_{solv}, associated with changes in hydration entropy; (ii) the conformational entropy change, ΔS_{conf}, accounting for the changes in conformational degrees of freedom; and (iii) the changes in rotational/translational degrees of freedom, ΔS_{rt} (*22*)

$$\Delta S(T) = \Delta S_{\mathrm{solv}}(T) + \Delta S_{\mathrm{conf}} + \Delta S_{\mathrm{rt}} \quad (14)$$

The entropy of solvation can be written in terms of the heat capacity change if the temperatures at which the apolar and polar hydration are zero ($T^*_{\mathrm{S,ap}} = 385.15$ K and $T^*_{\mathrm{S,pol}} = 335.15$ K) are used as reference temperatures (*25*, *32*)

$$\Delta S_{\mathrm{solv}}(T) = \Delta S_{\mathrm{solv,ap}} + \Delta S_{\mathrm{solv,pol}}(T) = \Delta C_{\mathrm{p,ap}} \ln\left(\frac{T}{T^*_{\mathrm{S,ap}}}\right) + \Delta C_{\mathrm{p,pol}} \ln\left(\frac{T}{T_{\mathrm{S,pol}}}\right) \quad (15)$$

Conformational entropy changes upon folding and/or oligomerization are evaluated by explicitly considering three different components (*25*, *33*)

$$\Delta S_{\mathrm{conf}} = \Delta S_{\mathrm{bu}\rightarrow\mathrm{ex}} + \Delta S_{\mathrm{ex}\rightarrow\mathrm{u}} + \Delta S_{\mathrm{bb}} \quad (16)$$

where $\Delta S_{\mathrm{bu}\rightarrow\mathrm{ex}}$ is the gain in conformational entropy of a side chain when it becomes exposed after disruption of tertiary and quaternary interactions, $\Delta S_{\mathrm{ex}\rightarrow\mathrm{u}}$ is the entropy change gained by a surface-exposed side chain when the peptide backbone itself unfolds, and ΔS_{bb} is the entropy gained by the backbone itself upon unfolding.

Finally, ΔS_{rt} takes into account the changes in translational and rotational degrees of freedom associated with the reaction because of the change in the number of particles in solution. This term seems to be well-accounted for by the cratic entropy (*22*), a statistical correction that reflects the mixing of solute and solvent molecules (*34*), as discussed by Kauzman (*35*). The change in mixing entropy for pentamer dissociation into monomers, using 1 M monomer as the standard state, is given by

$$\Delta S_{\mathrm{rt}} = \Delta S_{\mathrm{mix}} = \frac{1}{5}\left(4R \ln\left(\frac{1}{55.6}\right) + 5R \ln 5\right) = 3.19 \text{ cal K}^{-1} \text{ mol}^{-1} \quad (17)$$

Although the use of cratic entropy to estimate translational and rotational entropy and its physical basis is matter of controversy (*36*, *37*), recent experimental evidence (*38*, *39*), as well as theoretical arguments (*40*), has indicated that the loss/gain in rotational and translational entropy is numerically close to the cratic entropy. Therefore, we also used this approach to estimate the rotational and translational contribution to the overall entropy change upon pentamer unfolding.

For all the calculations described above, the accessible surface areas of the StxB pentamer as well as its isolated monomers were performed using Lee and Richards' solvent-accessibility algorithm (*41*), using a probe radius of 1.4 Å and a slice width of 0.25 Å.

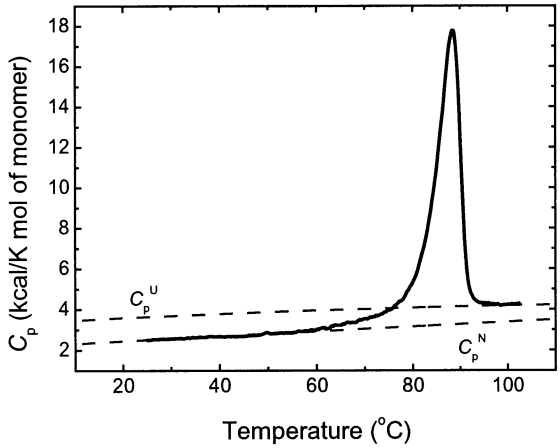

FIGURE 2: Partial molar heat capacity of STxB as function of temperature. STxB concentration in 10 mM HEPES (pH 7.0) was 265 μM monomers. The broken lines represent the heat capacities of the native (C_p^N) and unfolded (C_p^U) states, respectively, calculated in accordance with ref *23*.

RESULTS AND DISCUSSION

Differential Scanning Calorimetry. The thermal stability of STxB was measured by high-sensitivity differential scanning calorimetry. Figure 2 shows the partial molar heat capacity function of STxB at pH 7.0 and a protein concentration of 270 μM (here, STxB concentrations are always expressed in terms of monomer units). Under the conditions of this experiment, the thermally induced transition of STxB occurred at 88.5 °C and was characterized by an enthalpy change of 86 kcal mol^{-1} and a change in the heat capacity of 0.9 kcal K^{-1} mol^{-1}. At 25 °C, the heat capacity of the native state was 2.52 ± 0.06 kcal K^{-1} mol^{-1} or 0.328 ± 0.008 kcal K^{-1} g^{-1}, which is similar to the mean value of 0.34 ± 0.005 kcal K^{-1} g^{-1} for globular proteins (*18*, *23*). Figure 2 also shows that the heat capacities of both native and unfolded STxB are in good agreement with the values calculated using a structure-based parametrization (*23*). The similarity of the heat capacity of the unfolded STxB and the heat capacity expected for an unstructured polypeptide of the same sequence indicates that the polypeptide chain is essentially unfolded and hydrated after thermal denaturation.

The reversibility of the thermal denaturation of STxB was checked by examining the reproducibility of the calorimetric trace in a second heating of the same sample immediately after cooling from the first scan. It was observed (Figure 3) that when the calorimetric scans were interrupted immediately after the transition, the unfolding was fully reversible, indicating that the calorimetric experiments reflected equilibrium conditions. However, prolonged incu-

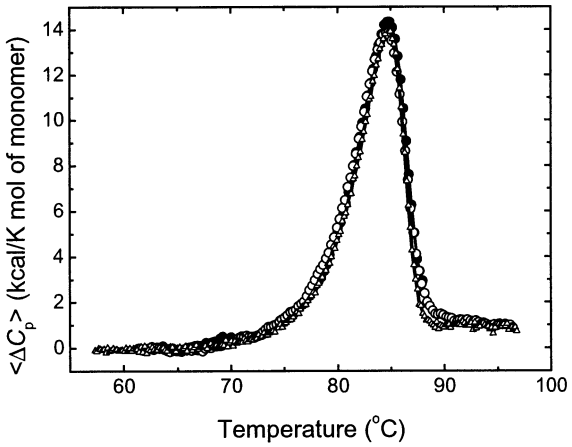

FIGURE 3: Demonstration of the reversibility and scan rate independence of the thermal unfolding of STxB. The figure depicts the excess heat capacity of STXB (79 μM) obtained at scan rate of 1 K min^{-1} (filled and open circles) and 0.34 K min^{-1} (open triangles). The curve labeled by filled circles represents the first scan, which was allowed to proceed up to a temperature at which the transition was 95% completed. The curve labeled by open circles is the second scan of that sample.

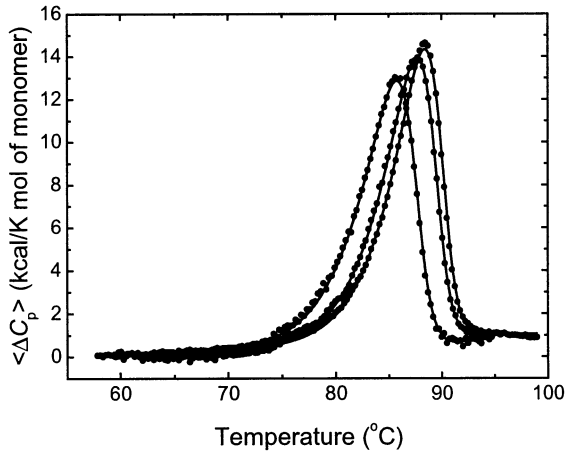

FIGURE 4: Excess heat capacity of STxB at different protein concentrations (115, 229, and 265 μM from left to right). The continuous lines represent theoretical curves generated with the two-state folding/unfolding coupled to oligomerization model and the best set of fitting parameters obtained by nonlinear least squares optimization. The thermodynamic parameters corresponding to the fits are presented in Table 1.

bation of STxB at high temperatures resulted in the appearance of the irreversibility. Thus, incubation of the toxin at 100 °C for longer than 5 min resulted in the preservation of approximately only 60% of the transitional enthalpy of the preceding scan. Experiments performed at scanning rates of 0.34 and 1 K min^{-1} gave practically the same denaturation profiles (see also Figure 3), indicating the absence of kinetic effects under the conditions of our experiments.

Owing to the pentameric nature of STxB, the stability of the native form is concentration-dependent (Figure 4). This figure shows the excess heat capacity functions obtained after subtracting the heat capacity of the native state. It may be seen that all transition peaks are skewed toward the low-temperature side of the transition, as expected for a transition coupled to dissociation according to eq 1 (*19*). Consequently, the temperature of the midpoint of the transition $T_{1/2}$ does not coincide with the temperature of the excess heat capacity maximum, T_m. For the calorimetric contours obtained for

Table 1: Thermodynamic Parameters for STxB Thermal Unfolding at pH 7[a]

[STxB] (μM)	T_m (°C)	$T_{1/2}$ (°C)	T_o[b] (°C)	ΔC_p (kcal K^{-1} mol^{-1})	ΔH(80 °C) (kcal mol^{-1})	ΔS(80 °C) (cal K^{-1} mol^{-1})	ΔG(80 °C) (kcal mol^{-1})
				DSC			
71.4	84.3	82.7	104.9	0.914	82.3	215.8	6.2
80.0	84.7	83.1	106.0	0.905	82.7	216.0	6.5
115.1	85.6	83.9	105.1	0.831	82.4	216.1	6.1
229.2	87.8	86.3	104.7	0.918	81.0	212.4	6.0
237.1	88.0	86.4	104.6	0.893	80.1	210.2	5.9
265.0	88.5	87.0	103.2	0.931	80.9	213.1	5.6
				CD			
4.2	76.5	75.4	115.2	0.9[c]	86.7	228.0	6.2
9.1	78.1	76.1	107.6	0.9[c]	80.3	209.2	6.4
18.6	80.7	79.6	110.7	0.9[c]	80.1	208.6	6.4
25.5	81.4	80.3	110.2	0.9[c]	83.7	219.5	6.2
34.7	82.3	81.2	108.7	0.9[c]	76.1	197.2	6.5

[a] The standard deviation for T_m and $T_{1/2}$ values is $\pm$0.2 K; the enthalpy of the unfolding was determined with standard deviation of $\pm$5%; ΔC_p is the difference between the heat capacities of the native and unfolded states obtained from the slope of the graph of the temperature-dependence of $\Delta H(T_m)$ by pH variation of T_m with the standard deviation of $\pm$0.015 kcal K^{-1} mol^{-1}. [b] T_o is the temperature value at which $\Delta G = \Delta H(T_o) + \Delta C_p(T - T_o) - T(\Delta S(T_o) + \Delta C_p \ln(T/T_o)) = 0$. [c] To fit the CD data, the value of ΔC_p was fixed.

different protein concentrations in this work, the ratio of the van't Hoff and calorimetric enthalpies ($\Delta H_{VH}/\Delta H$) obtained at a temperature where $\alpha = 0.5$ averaged 1.64 $\pm$ 0.07, which is reasonably close to the value calculated using the expression

$$\frac{\Delta H_{VH}}{\Delta H_{cal}} = \frac{2n}{n+1} \tag{18}$$

which is valid for the situation in which the unfolding of oligomeric proteins is coupled to their dissociation-unfolded monomers (*19*) (i.e., 1.67 for a pentamer).

The excess heat capacity functions obtained at different STxB concentrations were fitted individually to the two-state folding/unfolding oligomerization model (see lines through the data points in Figure 4) according to eq 8. Attempts to include intermediate forms in the fitting procedure did not improve the goodness of the fit, indicating that the two-state model is sufficient to describe the process quantitatively. The highest likelihood values for ΔH, ΔS, and ΔC_p obtained from fitting procedure are shown in Table 1.

CD Experiments. The far-UV CD spectra of native and thermally denatured STxB are shown in Figure 5. At 25 °C, the CD spectra are characteristic of an α/β protein (*42*), as expected from the crystallographic structure. Upon heating the samples to a temperature above thermal denaturation, the shape of the spectrum changes significantly, becoming characteristic of a random coil. Accordingly, the thermal denaturation of the STxB was monitored by following the changes in ellipticity at 225 nm since at this wavelength the changes in ellipticity are significant upon heating. In the insert of Figure 5 (symbols), the fractional degree of thermal unfolding of STxB as a function of temperature is shown for experiments carried out at different protein concentrations. As in the case of the DSC experiments, a displacement of the midpoint of the transition was observed as the protein concentration increased, indicating that the heat-induced conformational change in the protein produced changes in

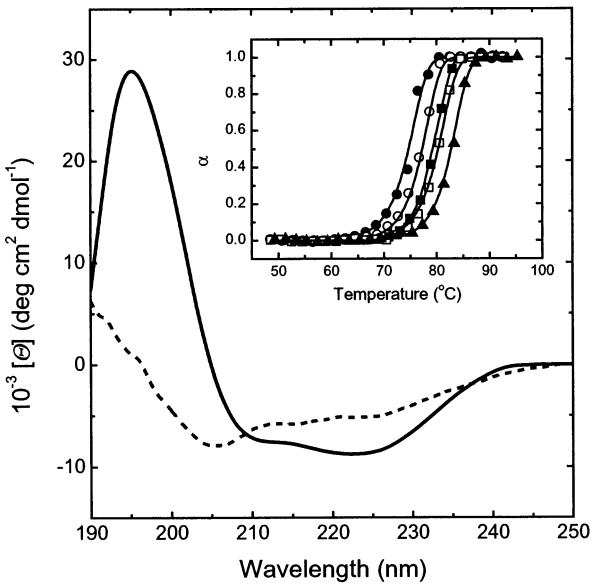

FIGURE 5: Far-UV spectra of STxB at 25 and 95 °C. Inset: Fractional degree of unfolding of STxB as a function of temperature monitored by the changes of ellipticity at 225 nm. The experiments were performed in 10 mM phosphate buffer (pH 7.0) at five different protein concentrations: 4 (filled circles), 9 (open circles), 19 (filled squares), 25 (open squares), and 35 (filled triangles) μM monomers. The continuous lines represent theoretical curves resulting from the fitting of the individual data sets to the two-state folding/unfolding coupled to oligomerization model.

its oligomerization state. The experimental data were analyzed as described above, assuming the simple model of a two-state protein unfolding coupled to oligomer dissociation. The lines through the data points in Figure 5 (insert) are the result of nonlinear least-squares fitting for individual data sets. The thermodynamic parameters obtained from the analysis of the CD experiments are also shown in Table 1. The magnitudes of the thermodynamic parameters characterizing STxB unfolding are similar to those obtained from DSC experiments, indicating that both techniques were monitoring the same process.

Concentration Dependence of STxB Stability. In Figure 6, the temperature of the maximum in the heat capacity function is plotted versus protein concentration. The continuous line represents the fit of the concentration dependence of the transition temperature for unfolding coupled to an association−dissociation equilibrium to the following mathematical relationship (*19*):

$$\frac{\Delta H(T_m)}{T_m} = \Delta S(T_m) + R\left[\left(1-\frac{1}{n}\right)\ln 2 - \frac{1}{n}\ln n\right] - R\left(1-\frac{1}{n}\right)\ln[C_o] \quad (19)$$

The fact that theoretical and experimental data are in a good agreement additionally testifies in favor of the model chosen for the analysis of STxB denaturation.

pH Dependence of STxB Stability. The pH dependence of the structural stability of STxB was examined by both DSC and CD techniques. Increasing the pH of the solution from 2.5 to 5 increased the conformational stability of StxB (as measured by its ΔG upon unfolding) from 7.5 to 13 kcal/mol, indicating that the unfolding reaction is coupled to an increase in the protonation state of the molecule. On the other hand, the structural stability of the protein decreased above neutral pH, indicating that the unfolding reaction is coupled to the release of protons in this pH range. The change in the Gibbs energy of stabilization with pH is proportional to the number of ionizable groups that become protonated/deprotonated (N) upon unfolding and can be determined by the thermodynamic formula:

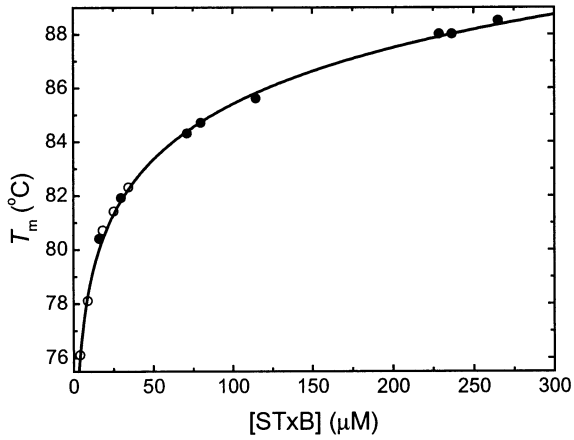

FIGURE 6: Unfolding transition temperature of STxB as a function of protein concentration. Open circles represent temperatures at which the rate of change of STxB ellipticity at 225 nm with temperature is maximum, while filled circles represent the temperature of the maximum in the heat capacity curve versus protein concentration. The continuous line is a logarithmic fit through the data points in accordance to eq 19.

$$\frac{\partial \Delta G}{\partial \mathrm{pH}} = 2.303RTN \quad (20)$$

According to a simple binding model for protonation/deprotonation (see for details ref *43*), the pH dependence of the Gibbs energy change of an unfolding process can be written as

$$\Delta G = \Delta G^{\circ} - RTN \ln\left[\frac{1+10^{\mathrm{p}K_u - \mathrm{pH}}}{1+10^{\mathrm{p}K_n - \mathrm{pH}}}\right] \quad (21)$$

where ΔG° is the value of ΔG at the reference pH, and pK_n and pK_u are the apparent pK of ionizable groups in the native and unfolded states, respectively. The pH dependence of the free-energy change upon STxB unfolding is shown in Figure 7. Analysis of the data indicates that on average two groups per monomer become protonated in the acidic range at pH 3.5, while two groups per monomer become deprotonated in the alkaline range at pH 10 (Figure 7B) upon protein unfolding. The apparent pK of those groups was estimated to be in the order of 4.7 and 9.1 in the unfolded state, and 2.3 and 10.7 in the native state, indicating that the groups responsible for the pH dependence of STxB stability are carboxylic groups in the acid region, of which the STxB pentamer has 40 (25 Asp and 15 Glu) and that alkali denaturation is triggered by deprotonation of Lys residues, most probably Lys13 (Figure 1).

Gdn-HCl Dependence of STxB Stability at 25 °C. The Gdn-HCl dependence of STxB stability was measured by monitoring CD ellipticity at 225 nm (Figure 8). The experimental data obtained at constant temperature of 25 °C and at pH 7 were fitted to the same two-state folding/unfolding oligomerization model that was used to fit the heat-

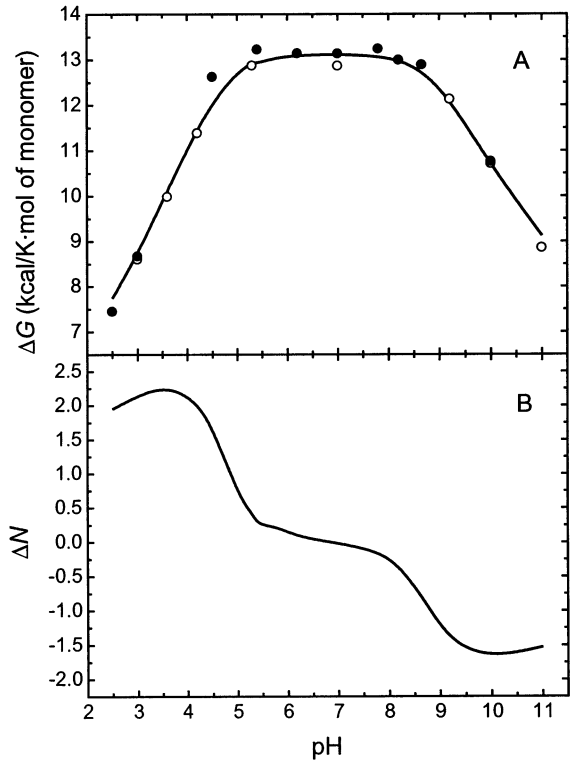

FIGURE 7: (A) pH dependence of Gibbs energy change as determined by DSC (filled circles) and CD (open circles). The fitted curve (eq 21) was generated with $N = 2$, $pK_u = 4.7$, and $pK_d = 2.3$ for the pH region from 2.5−7 and with $N = 2$, $pK_u = 9.1$, and $pK_d = 10.7$ for the pH region from 7 to 11. (B) Proton flux N was involved in unfolding of STxB as a function of pH. The curve was obtained by numerical differentiation of the data shown in panel A employing eq 20.

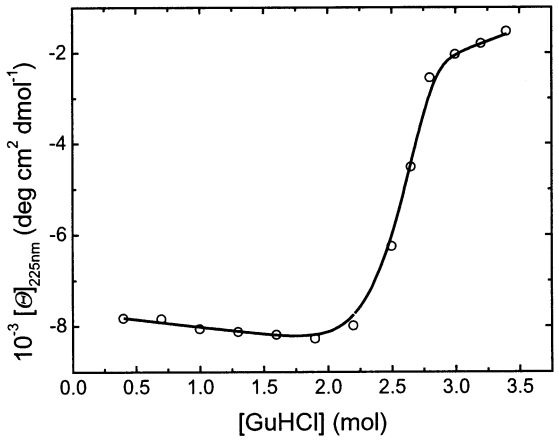

FIGURE 8: Ellipticity of the STxB at 225 nm as a function of the Gdn-HCl concentration. STxB was equilibrated in 10 mM phosphate buffer, pH 7.0, plus Gdn-HCl for 30−60 min at 25 °C, the establishment of equilibrium conditions being confirmed by measuring the rate of equilibration. Aliquots were refolded after 2 h to check for reversibility, which was more than 90%. The continuous line is the best fit using the two-state folding/unfolding coupled oligomerization model.

induced unfolding of the protein monitored using both DSC and CD data. In this case, the dependence of ΔG on the Gdn-HCl concentration was analyzed in terms of the linear extrapolation method (*44*)

$$\Delta G = \Delta G(H_2O) - m[\text{Gnd-HCl}] \qquad (22)$$

Table 2: Dissection of Folding Energetics of STxB Pentamer at 25 and 80 °C[a]

parameter	monomer folding $U \overset{K}{\leftrightarrow} N$	oligomerization $N \overset{K}{\leftrightarrow} \frac{1}{5}N_5$	global $U \overset{K}{\leftrightarrow} \frac{1}{5}N_5$
ΔASA_{ap} (Å^2)	−3699.7	−778.2	−4477.9
ΔASA_{pol} (Å^2)	−2536.8	−421.8	−2958.6
ΔC_p (cal K^{-1} mol^{-1})	−1005.3	−240.6	−1245.9
ΔH (kcal mol^{-1}, 25 °C)	−13.2	1.7	−11.5
ΔS_{conf} (cal K^{-1} mol^{-1})	−401.8	−22.9	−424.7
ΔS_{solv} (cal K^{-1} mol^{-1}, 25 °C)	349.1	76.8	425.9
ΔS_{rt} (cal K^{-1} mol^{-1})	0.0	−3.2	−3.2
ΔS_{total} (cal K^{-1} mol^{-1}, 25 °C)	−52.6	50.7	−1.9
$-T\Delta S_{total}$ (kcal mol^{-1}, 25 °C)	15.7	−15.1	0.6
ΔG_{total} (kcal mol^{-1}, 25 °C)	2.5	−13.4	−10.9
ΔH (kcal mol^{-1}, 80 °C)	−68.5	−11.5	−80.0
ΔS_{conf} (cal K^{-1} mol^{-1})	−401.8	−22.9	−424.7
ΔS_{solv} (cal K^{-1} mol^{-1}, 80 °C)	178.9	36.1	215.0
ΔS_{rt} (cal K^{-1} mol^{-1})	0.0	−3.2	−3.2
ΔS_{total} (cal K^{-1} mol^{-1}, 80 °C)	−222.8	10.0	−212.8
$-T\Delta S_{total}$ (kcal mol^{-1}, 80 °C)	78.7	−3.5	75.2
ΔG_{total} (kcal mol^{-1}, 80 °C)	10.2	−15.0	−4.8

[a] Thermodynamic parameters and ASA values are reported per monomer. The native conformation is the reference state.

where $\Delta G(H_2O)$ is the Gibbs energy change in the absence of denaturant, and m is a measure of the observed linear dependence of ΔG on the Gnd-HCl concentration.

As shown in Figure 8, this model offers a good explanation of the Gnd-HCl denaturation data. The m value is 3.1 ± 0.1 kcal mol^{-1} [Gnd-HCl]$^{-1}$ (i.e., close to that observed for other proteins of similar molecular weight (*45*)). The conformation stability of the protein, $\Delta G(H_2O)$, at 25 °C is 13.0 ± 0.1 kcal mol^{-1}, in close agreement with the ΔG value extrapolated from the thermodynamic parameters obtained from the heat-induced unfolding experiments monitored by CD and DSC.

Therefore, the results of both the chemical and the thermal denaturation experiments are in agreement with a two-state model in which the population of folded monomers throughout the transition is negligible, and only pentamers and unfolded monomers are significantly populated.

Structure-Based Dissection of the Structural Stability of STxB. Taking the crystal structure of STxB solved at 2.50 Å resolution (*15*) as a template, we carried out structure-based thermodynamic calculations using the methodology developed by Freire et al., as briefly explained in the Materials and Methods. The main reason for performing such calculations was to dissect the overall energetics upon pentamer folding into the different enthalpic and entropic components, as well as to analyze the energetic contributions coming from intramolecular and intermolecular interactions (i.e., isolated monomer stability as opposed to the oligomerization of folded monomers).

Table 2 summarizes the results of the structural thermodynamic calculations. The thermodynamic parameters predicted by the structure-based calculations are in good agreement with the experimental ones (see Table 1) at 80 °C. The concentration-independent enthalpy, entropy, and free energy changes upon the folding of isolated STxB monomers into their pentameric structure are predicted to be −80 kcal mol^{-1}, −212.8 cal K^{-1} mol^{-1}, and −4.8 kcal mol^{-1}, respectively, in close agreement with the experimental

values determined for the reverse reaction (unfolding of STxB pentamer).

These calculations reveal that in agreement with the experimental results reported above, isolated folded monomers are not energetically favorable, and consequently their population is negligible in the 0−100 °C temperature range. At 25 °C, the favorable enthalpic contribution to the free energy change upon isolated monomer folding (−13.2 kcal mol^{-1}) is overcome by the large and unfavorable entropic contribution ($-T\Delta S = 15.7$ kcal mol^{-1}), which justifies the endergonic nature of the folding reaction ($\Delta G = 2.5$ kcal mol^{-1}) and therefore explains the intrinsic instability of the monomeric structure. Furthermore, the entropic penalty coming from the reduction in conformational freedom upon monomer folding (−401.8 cal K^{-1} mol^{-1}) is not compensated by the gain in solvent entropy induced by dehydration of solvent-accessible protein groups in the unfolded monomer folding (349.1 cal K^{-1} mol^{-1}). It is thus possible to rationalize the conformational instability of isolated STxB monomers as being due to exposure to the solvent of a large amount of apolar groups that only become buried upon oligomerization.

Although the formation of a substantial hydrophobic core upon monomer folding accounts for the gain of almost 82% in the total solvent entropy for the folding of the pentamer (arising mainly from the release of water molecules upon burial of hydrophobic surfaces), the internal van der Waals and hydrogen bonding interactions established within the folded monomer are not strong enough to compensate for the large decrease in conformational entropy because of the restrictions imposed by the folded conformation to both the monomer backbone and the side chains.

The oligomerization of isolated STxB monomers is highly exergonic at both 25 and 80 °C (−13.4 and −15.0 kcal mol^{-1}, respectively). The energetically favorable intersubunit interactions overcome the adverse free energy change upon monomer folding and are therefore primarily responsible for the conformational stability of the pentameric structure of STxB. Structurally, the interface between individual monomers in the complex is very hydrophobic (65% of the interacting surfaces contain apolar groups). The association of folded monomers does not involve a high entropic penalty (−22.9 cal K^{-1} mol^{-1} coming from conformational change and 3.2 cal K^{-1} mol^{-1} from the reduction in rotation and translation degrees of freedom), while desolvation of the interacting groups (mainly apolar) becomes entropically favorable (76.8 cal K^{-1} mol^{-1}).

In summary, structure-based thermodynamic calculations allow one to dissect the overall folding energetics of STxB folding from unfolded monomers into its final pentameric structure in terms of two independent processes: the folding of individual monomers and their subsequent oligomerization. These calculations rationalize the experimental observation that only folded pentamer and unfolded monomers are significantly populated along the folding/unfolding equilibrium. The fact that these calculations predict that isolated folded monomers are energetically unfavorable argues in favor of the two-state unfolding model used to fit the experimental data.

CONCLUSION

In this paper, we have demonstrated that the thermal unfolding of STxB is a two-state process in which the folded pentamer unfolds cooperatively into unfolded monomers. Under all conditions studied, the concentration of intermediate species could not be detected calorimetrically. Also, the CD data are consistent with the presence of only two significantly populated states.

Structure-based thermodynamic calculations of the thermodynamic parameters of STxB unfolding yields ΔG, ΔH, and ΔC_p values that are in general agreement with the experimental values. The lack of stability of isolated monomers appears to be due to the absence of tight van der Waals contacts and the burial of a significant part of the surface from the solvent. The results obtained with STxB emphasize the dominating role of quaternary interactions in the stabilization of small oligomeric proteins (*46*−*48*).

ACKNOWLEDGMENT

We thank Dr. F. Gavilanes from the Universidad Complutense de Madrid, Spain, for CD experimental facilities; Dr. J. M. Sanchez-Ruiz from Granada University, Spain, for valuable suggestions; Drs. A. Saint-Pol and C. Lamaze from the Institut Curie, Paris, for fruitful discussions; and L. Cabanie for technical assistance.

REFERENCES

1. Falnes, P. O., and Sandvig, K. (2000) Penetration of protein toxins into cells, *Curr. Opin. Cell Biol. 12*, 407−413.
2. Sandvig, K., and van Deurs, B. (1996) Endocytosis, intracellular transport, and cytotoxic action of Shiga toxin and ricin, *Physiol. Rev. 76*, 949−966.
3. Donohue-Rolfe, A., Jacewicz, M., and Keusch, G. T. (1989) Isolation and characterization of functional Shiga toxin subunits and renatured holotoxin, *Mol. Microbiol. 3*, 1231−1236.
4. Nichols, B. J., Kenworthy, A. K., Polishchuk, R. S., Lodge, R., Roberts, T. H., Hirschberg, K., Phair, R. D., and Lippincott-Schwartz, J. (2001) Rapid cycling of lipid raft markers between the cell surface and Golgi complex, *J. Cell Biol. 153*, 529−541.
5. Sandvig, K., Olsnes, S., Brown, J. E., Petersen, O. W. and van Deurs, B. (1989) Endocytosis from coated pits of Shiga toxin: a glycolipid-binding protein from *Shigella dysenteriae* 1, *J. Cell Biol. 108*, 1331−1343.
6. Sandvig, K., Garred, O., Prydz, K., Kozlov, J. V., Hansen, S. H., and van Deurs, B. (1992) Retrograde transport of endocytosed Shiga toxin to the endoplasmic reticulum, *Nature 358*, 510−512.
7. Johannes, L., and Goud, B. (1998) Surfing on a retrograde wave: how does Shiga toxin reach the endoplasmic reticulum? *Trends Cell Biol. 8*, 158−162.
8. Johannes, L. (2002) The epithelial cell cytoskeleton and intracellular trafficking I. Shiga toxin B-subunit system: retrograde transport, intracellular vectorization, and more, *Am. J. Physiol.: Gastrointest. Liver Physiol. 283*, G1−G7.
9. Sandvig, K., and van Deurs, B. (2002) Transport of protein toxins into cells: pathways used by ricin, cholera toxin, and Shiga toxin, *FEBS Lett. 529*, 49−53.
10. Hazes, B., and Read, R. J. (1997) Accumulating evidence suggests that several AB-toxins subvert the endoplasmic reticulum-associated protein degradation pathway to enter target cells, *Biochemistry 36*, 11051−11054.
11. Wesche, J., Rapak, A., and Olsnes, S. (1999) Dependence of ricin toxicity on translocation of the ricin A-chain from the endoplasmic reticulum to the cytosol, *J. Biol. Chem. 274*, 34443−34449.
12. Haicheur, N., Bismuth, E., Bosset, S., Adotevi, O., Warnier, G., Lacabanne, V., Regnault, A., Desaymard, C., Amigorena, S., Riccardi-Castagnoli, P., Goud, B., Fridman, W. H., Johannes, L., and Tartour, E. (2000) The B-subunit of Shiga toxin fused to a tumor antigen elicits CTL and targets dendritic cells to allow MHC class I restricted presentation of peptides derived from exogenous antigens, *J. Immunol. 165*, 3301−3308.
13. Stein, P. E., Boodhoo, A., Tyrell, G. J., Brunton, J. L., and Read, R. J. (1992) Crystal structure of the cell-binding B oligomer of verotoxin-1 from *Escherichia coli*, *Nature 355*, 748−750.

14. Richardson, J. M., Evans, P. D., Homans, S. W., and Donohue-Rolfe, A. (1997) Solution structure of the carbohydrate-binding B-subunit homopentamer of verotoxin VT-1 from *Escherichia coli*, *Nat. Struct. Biol. 4*, 190−193.
15. Fraser, M. E., Chernaya, M. M., Kozlov, Y. V., and James, M. N. (1994) Crystal structure of the holotoxin from *Shigella dysenteriae* at 2.5 Å resolution, *Nat. Struct. Biol. 1*, 59−64.
16. Ling, H., Boodhoo, A., Hazes, B., Cummings, M. D., Armstrong, G. D., Brunton, J. L., and Read, R. J. (1998) Structure of the Shiga-like toxin I B-pentamer complexed with an analogue of its receptor Gb_3, *Biochemistry 37*, 1777−1788.
17. Shimizu, H., Field, R. A., Homans, S. W., and Donohue-Rolfe, A. (1998) Solution structure of the complex between the B-subunit homopentamer of verotoxin VT-1 from *Escherichia coli* and the trisaccharide moiety of globotriaosylceramide, *Biochemistry 37*, 11078−11082.
18. Privalov, P. L. (1979) Stability of proteins: small globular proteins, *Adv. Protein Chem. 33*, 167−239.
19. Freire, E. (1989) Statistical thermodynamic analysis of the heat capacity function associated with protein folding−unfolding transitions, *Comm. Mol. Cell Biophys. 6*, 123−140.
20. Freire, E. (1995) Thermal denaturation methods in the study of protein folding, *Methods Enzymol. 259*, 145−168.
21. Sanchez-Ruiz, J. M. (1995) Differential scanning calorimetry of proteins, in *Subcellular Biochemistry 24. Proteins: structure, function and engineering* (Biswas, B. B., and Siddhartha, R., Eds.) pp 133−166, Plenum Press, New York.
22. Gómez, J., and Freire, E. (1995) Thermodynamic mapping of the inhibitor binding site of the aspartic protease endothiapepsin, *J. Mol. Biol. 252*, 337−350.
23. Gómez, J., Hilser, V. J., Xie, D., and Freire, E. (1995) The heat capacity of proteins, *Proteins: Struct., Funct., Genet. 22*, 404−412.
24. Hilser, V. J., Gómez, J., and Freire, E. (1996) The enthalpy change in protein folding and binding: refinement of parameters for structure-based calculations, *Proteins: Struct., Funct., Genet. 26*, 123−133.
25. D′Aquino, J. A., Gómez, J., Hilser, V. J., Lee, K. H., Amzel, M. L., and Freire, E. (1996) The magnitude of the backbone conformational entropy change in protein folding, *Proteins: Struct., Funct., Genet. 25*, 143−156.
26. Johannes, L., Tenza, D., Antony, C., and Goud, B. (1997) Retrograde transport of KDEL-bearing B-fragment of Shiga toxin, *J. Biol. Chem. 272*, 19554−19561.
27. Saleh, M. T., and Gariepy, J. (1993) Local conformational change in the B-subunit of Shiga-like toxin 1 at endosomal pH, *Biochemistry 32*, 918−922.
28. Shnyrov, V. L., Villar, E., Zhadan, G. G., Sanchez-Ruiz, J. M., Quintas, A., Saraiva, M. J. M., and Brito, R. M. M. (2000) Comparative calorimetric study of nonamyloidogenic and amyloidogenic variants of the homotetrameric protein transthyretin, *Biophys. Chem. 88*, 61−67.
29. Murphy, K. P., and Freire, E. (1992) Thermodynamics of structural stability and cooperativity of folding behavior in proteins, *Adv. Protein Chem. 43*, 313−361.
30. Spolar, R. S., Livingstone, J. R., and Record, M. T., Jr. (1992) Use of liquid hydrocarbon and amide transfer data to estimate contributions to thermodynamic functions of protein folding from the removal of nonpolar and polar surface from water, *Biochemistry 31*, 3947−3955.
31. Baker, B. M., and Murphy, K. P. (1997) Prediction of binding energetics of a protein−protein interaction: The binding of ovomucoid third domain to elastase, *J. Mol. Boil. 268*, 557−569.
32. Baldwin, R. L. (1986) Temperature dependence of the hydrophobic interaction in protein folding, *Proc. Natl. Acad. Sci. U.S.A. 83*, 8069−8072.
33. Lee, K. H., Xie, D., Freire, E., and Amzel, L. M. (1994) Estimation of changes in side chain configurational entropy in binding and folding: general methods and application to helix formation, *Proteins 20*, 68−84.
34. Gurney, R. W. (1953) *Ionic Processes in Solution*, McGraw-Hill, New York.
35. Kauzman, W. (1959) Some factors in the interpretation of protein denaturation, *Adv. Protein Chem. 14*, 1−63.
36. Holtzer, A. (1995) The "cratic correction" and related fallacies, *Biopolymers 35*, 595−602.
37. Gilson, M. K., Given, J. A., Bus, B. L., and McCammon, J. A. (1997) The statistical-thermodynamic basis for computation of binding affinities: a critical review, *Biophys J. 72*, 1047−1069.
38. Tamura, A., and Privalov, P. L. (1997). The entropy of protein association, *J. Mol. Biol.* 273, 1048−1060.
39. Yu, Y., Lavigne, P., Kay, C. M., Hodges, R. S., and Privalov, P. L. (1998) Contribution of translational and rotational entropy to the unfolding of a dimeric coiled−coil, *J. Phys. Chem. B 103*, 2270−2278.
40. Amzel, L. M. (1996) Loss of translational entropy in binding, folding, and catalysis, *Proteins: Struct., Funct., Genet. 29*, 1−6.
41. Lee, B., and Richards, F. M. (1971) The interpretation of protein structures: estimation of static accessibility, *J. Mol. Biol. 55*, 379−400.
42. Venyaminov, S. Y., and Vasilenko, K. S. (1994) Determination of protein tertiary structure class from circular dichroism spectra, *Anal. Biochem. 222*, 176−184.
43. Wyman, J., and Gill, S. J. (1990) *Binding and Linkage*, pp 1−330, University Science Books, Mill Valley, CA.
44. Greene, R. F., and Pace, C. N. (1974) Urea and guanidine hydrochloride denaturation of ribonuclease, lysozyme, α-chymotrypsin, and β-lactoglobulin, *J. Biol. Chem. 249*, 5388−5393.
45. Myers, J. K., Pace, C. N., and Scholtz, J. M. (1995) Denaturant *m* values and heat capacity changes: Relation to changes in accessible surface areas of protein unfolding, *Protein Sci. 4*, 2138−2148.
46. Johnson, C. R., Morin, P. E., Arrowsmith, C. H., and Freire, E. (1995) Thermodynamic analysis of the structural stability of the tetrameric oligomerization domain of p53 tumor suppressor, *Biochemistry 34*, 5309−5316.
47. Kenar, K. T., García-Moreno, B., and Freire, E. (1995) A calorimetric characterization of the salt dependence of the stability of the GCN4 leucine zipper, *Protein Sci. 4*, 1934−1938.
48. Boudker, O., Todd, M. J., and Freire, E. (1997) The structural stability of the co-chaperonin GroES, *J. Mol. Biol. 272*, 770−779.

BI034591S